# Sensitivity of Robust Flutter Boundary to Model Uncertainties in Aeroservoelastic Systems

Aditya Kotikalpudi,* Harald Pfifer† and Peter Seiler‡

*Department of Aerospace Engineering & Mechanics*

*University of Minnesota, Minneapolis, MN, 55414, USA*

**The dynamics of a flexible air vehicle are typically described using an aeroservoelastic model which accounts for interaction between aerodynamics, structural dynamics, rigid body dynamics and control laws. These subsystems are individually modeled using a combination of theory and experimental data from various ground tests. For instance, the structural dynamics model can be obtained using a finite element method which is then updated using data from ground vibration tests. Similarly, an aerodynamic model can be obtained from linear panel methods or computational fluid dynamics and updated using data from wind tunnel tests. In all cases, the models obtained for the subsystems have a degree of uncertainty owing to inherent assumptions in the theory and errors in experimental data. By suitably modeling these uncertainties, a robust stability analysis may be carried out to obtain a robust flutter boundary. In this paper, we examine the affects of bounds on various uncertainties on the resulting robust flutter boundary. This analysis helps us deduce the subsystems most important for a good flutter prediction.**

## I. Introduction

Aeroservoelastic systems are increasingly gaining prominence in flight dynamics modeling and control design due to use of highly flexible light-weight materials for construction of modern aircraft. The interaction between structural dynamics, aerodynamics, rigid body dynamics and control laws of such aircraft can lead to unstable phenomena like flutter.[1,2] To capture these instabilities in a flight dynamics model, it is necessary to develop dependable methods for modeling aeroservoelastic effects as accurately as possible. The resulting models may have additional requirement constraints such as linearity and low number of states for control design.

The Unmanned Aerial Vehicles (UAV) research group at the University of Minnesota carries out extensive research in the field of aeroservoelastic systems. Theoretical research in system modeling,[3,4] model reduction[5,6] and control design[7,8] is supplemented by experimental work in ground vibration tests,[9,10] flight tests[11] and system identification.[12,13] The group maintains a well equipped UAV laboratory for experimental research and flight tests. The group is also a part of a multi-disciplinary, multi-institutional team of researchers from academia and industry, working on a grant from NASA titled the Performance Adaptive Aeroelastic Wing (`www.paaw.net`) (see acknowledgments). The objective is to demonstrate flutter suppression and active morphing wing control in flight. The group has built a number of test bed UAVs with varying structural characteristics for this purpose[14] and has begun conducting flight tests. In keeping with the research philosophy of the group, all data related to flight and ground tests, modeling tools and control design tools are made open source on the group website mentioned above.

The underlying need for all these areas of research are reliable and control design oriented models. A common approach to constructing these models is by describing the overall system as an interconnection between various subsystems as shown in Fig. 2. Each of the subsystems is individually modeled in a common coordinate system for ease of interconnections. A significant advantage of this approach is the flexibility offered in choosing the modeling technique and fidelity for each subsystem. For instance, the structural

*Graduate Student, AIAA Student Member

†Postdoctoral Associate

‡Assistant Professor

model could be constructed using nonlinear beam theory while the aerodynamics could be modeled using linear potential flow theory. However, it is important to note that every method involves certain assumptions which lead to modeling errors in the subsystem. Hence, it is important to account for these inherent errors in the overall system for a robust analysis for flutter instabilities and robust control design.

The structured singular value ($\mu$) is a widely used measure of robust stability for systems with predefined uncertainties. A short summary of $\mu$ analysis[15,16] is provided in section III. The uncertainties considered can range from unmodeled high frequency dynamics to parametric errors in the model. The $\mu$ based framework has also been used in recent years to carry out robust flutter analysis for aeroservoelastic systems.[17,18] Lind and Brenner have also demonstrated the method for updating model uncertainties using flight data, both offline and in real time during flight.[19] However, the relative effects of different sources of uncertainties on these analyses has not been explored as much using this framework. Such an analysis is considered in this paper and requires a skewed-$\mu$ calculation.[20,21] It should be noted that a more general approach for representing modeling errors, called the Integral Quadratic Constraints (IQCs), are also used as a framework for flutter analysis[22–24] which accounts for various nonlinearities in the model in addition to the above mentioned uncertainties.

In this paper we look at a sensitivity analysis using the $\mu$ framework where the effects of different modeling errors on flutter prediction are quantified in an individual capacity. The nominal aeroelastic model is developed using the subsystem approach mentioned earlier, as described in Section II. The uncertainties are modeled in a structured manner and their bounds are based on estimates of measurement errors and theoretical approximations (see Section III). The structured nature of the uncertainties makes it possible to carry out flutter analysis with each uncertainty scaled independently of another (see Section IV). Finally, the results of this analysis provides insights on the required fidelity of the corresponding subsystems which in turn would help choose the appropriate methods for their modeling (Section IV).

## II. Aeroelastic Model

In this section, the basic aeroelastic model used in this paper is described. The uncertain model described in the later sections uses this as the nominal model. The aircraft chosen for aeroelastic modeling is the Body Freedom Flutter (BFF) vehicle, see Fig 1. The BFF vehicle was developed by the Lockheed Martin (LM) and the Air Force Research Lab as a testbed for their flutter suppression control laws.[25] The aircraft exhibits the so called body freedom flutter, in which the first wing bending mode couples with the rigid short period mode to create instability which can lead to loss of aircraft. Indeed several aircraft were lost during research testing as LM attempted to push beyond the (open-loop) flutter boundary using advanced controls. The last version was generously donated to the University of Minnesota UAV research group. The aerodynamic design of the test beds constructed by the UAV research group is based on the BFF vehicle.

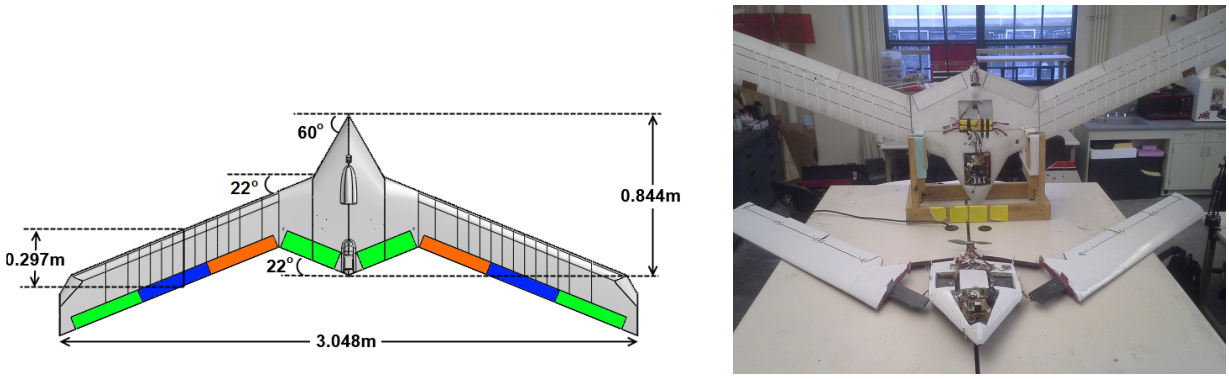


(a) BFF Design

(b) BFF and miniMUTT

**Figure 1. Body Freedom Flutter Vehicle (background) with the rigid body version built by UMN**

The image in Fig. 1(b) shows the BFF vehicle in the background. The foreground shows a rigid version of the aircraft built in-house by the group, named the mini-MUTT. The airframe has been designed to have detachable wings, which allows for wings of variable flexibility to be attached to the center body. This

concept is based on the X-56A MUTT test bed developed by NASA[26] and allows for testing a range of test beds with varying flexibility. Since the aerodynamic design remains same across these test beds, the modular subsystem based approach used in this paper can efficiently model them by simply modifying the structural dynamics subsystem. The model is conceptually described in Fig. 2 and the modeling process for subsystems is discussed further.

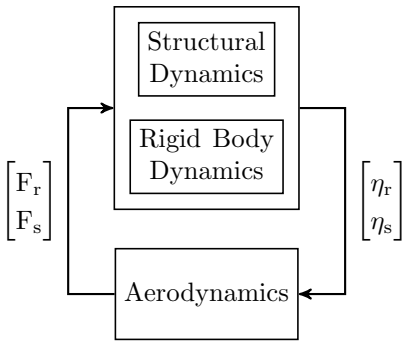


**Figure 2. Nominal Aeroelastic Model**

## A. Rigid Body Dynamics

The rigid body dynamics are developed for all six degrees of freedom about the so called mean axes.[27] The mean axes formulation allows for the inertial decoupling of rigid body dynamics from the structural dynamics assuming small deformations. Hence, rigid body forces and the resulting displacements can be handled as done in classical flight dynamics. The mass properties such as center of mass location and moments of inertia are obtained experimentally. The measurement errors in these experiments have been carefully estimated to serve as a basis for bounding the associated uncertainties. The nonlinear equations for rigid body dynamics are

$$\begin{bmatrix} m(\dot{V}_r(t) + \Omega_r(t) \times V_r(t) - T_g g) \\ I_r \dot{\Omega}_r(t) + \Omega_r(t) \times I_r \Omega_r(t) \end{bmatrix} = F_r(t) \tag{1}$$

Here $m, I_r$ are the mass and moments of inertia of the aircraft. $V_r, \Omega_r$ represent the translational and angular velocities in the mean axes with respect to inertial axes. $F_r$ represents forces and moments along the mean axes and $T_g$ is the rotation matrix from inertial to mean axes. Referring to Fig. 2, we see that the rigid body modes are $\eta_r = \begin{bmatrix} V_r \\ \Omega_r \end{bmatrix}$. The mass properties of the aircraft are listed in Table 1.

**Table 1. Mass Properties**

| Property | Value |
|---|---|
| Total mass | 5.42 kg |
| CG location | 0.59 m (from nose) |
| Pitching moment of inertia | 0.36 kg m$^2$ |
| Rolling moment of inertia | 2.50 kg m$^2$ |
| Yawing moment of inertia | 2.37 kg m$^2$ |

## B. Structural Dynamics

The structural model is developed using a finite element method which consists of linear Euler beam elements.[9,10] The beams are interconnected as shown in Fig. 3. The model has 14 nodes interconnected with beams which have 3 degrees of freedom - heave, twist and bending. This makes the total number of degrees

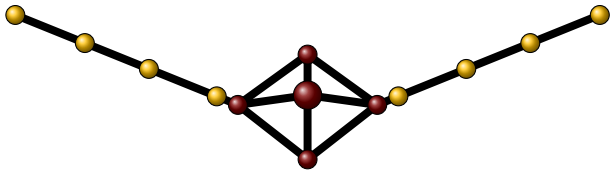

**Figure 3. Finite Element Model for the BFF Vehicle**

of freedom 42. Modal decomposition is carried out to transform the system into decoupled modal coordinates. It is then possible reduce the degrees of freedom via modal truncation.[28] Only the first 12 modes are retained and all the higher frequency modes are truncated from the model.[9] The final mathematical form of the model in modal coordinates is written as

$$M_s\ddot{\eta}_s(t) + C_s\dot{\eta}_s(t) + K_s\eta_s(t) = F_s(t) \tag{2}$$

Here $M_s, C_s$ and $K_s$ are the modal mass, damping and stiffness matrices and $\eta_s$ is the modal coordinates vector. The material properties associated with stiffness, Young's modulus and Shear modulus, are estimated via static tests as well as ground vibration tests.[9,10] The experimental errors in their measurements contribute to modeling uncertainties. Equation (1), which represents nonlinear rigid body dynamics, can be linearized about a given trim condition and combined the linear structural model in Eq. (2). The mean axes formulation ensures that the rigid body modes are orthogonal and therefore decoupled from the structural dynamics modes. The combined dynamics can be written as

$$\begin{aligned} &M\begin{bmatrix}\ddot{\eta}_r(t)\\ \ddot{\eta}_s(t)\end{bmatrix} + C\begin{bmatrix}\dot{\eta}_r(t)\\ \dot{\eta}_s(t)\end{bmatrix} + K\begin{bmatrix}\eta_r(t)\\ \eta_s(t)\end{bmatrix} = \begin{bmatrix}F_r(t)\\ F_s(t)\end{bmatrix}\\ &M = \begin{bmatrix}M_r & 0\\ 0 & M_s\end{bmatrix}, \quad C = \begin{bmatrix}0 & 0\\ 0 & C_s\end{bmatrix}\\ &K = \begin{bmatrix}0 & 0\\ 0 & K_s\end{bmatrix}, \quad M_r = \begin{bmatrix}mI_{3\times3} & 0\\ 0 & I_r\end{bmatrix} \end{aligned} \tag{3}$$

### C. Aerodynamics

In an aircraft undergoing structural vibrations in flight, unsteady aerodynamic effects can potentially play a significant role in inducing instabilities. Unsteady effects come into play since it takes a finite amount of time for aerodynamic forces to redistribute around the aircraft as it deforms in flight. To account for the resulting lag effects, a potential flow based panel method known as the doublet lattice method (DLM) has been implemented,[29,30] along with a standard vortex lattice method (VLM) to take care of the steady part.[3] Fig. 4 shows the aerodynamic panels for the BFF vehicle.

The DLM provides solutions for lifting surfaces undergoing simple harmonic oscillations at a given frequency $\omega$ and a given airspeed $V$. Specifically, the solution is obtained for a given dimensionless reduced frequency defined as $k := \omega\frac{c_{\text{ref}}}{2V}$ where $c_{\text{ref}}$ is the reference chord. Suitable coordinate transformations are carried out to express the model in structural modal coordinates as

$$\begin{bmatrix}F_r\\ F_s\end{bmatrix} = \bar{q}A(ik)\begin{bmatrix}\eta_r\\ \eta_s\end{bmatrix} \tag{4}$$

where $\bar{q}$ is the dynamic pressure. $A(ik)$ is a complex valued matrix obtained as a solution from the DLM for a given $k$. Since it is only obtained at discrete values of the reduced frequency, a least squares fit is carried out for a set of solutions over a predefined rational function. The rational function chosen for this purpose is the Roger's approximation.[31] The continuous model is expressed in terms of the reduced frequency Laplace

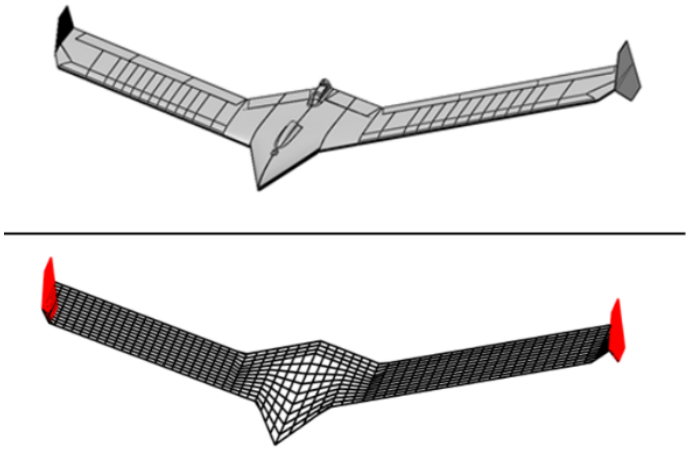

**Figure 4. Aerodynamic Model for the BFF Vehicle**

variable $s_r$ as

$$A(s_r) = \left( \underbrace{A_0 + A_{1s} s_r}_{\text{steady aero}} + \underbrace{A_{1us} s_r + A_2 (s_r)^2 + \overbrace{\sum_{l=1}^{n} A_l \frac{s_r}{s_r + b_l}}^{\text{aero lag terms}}}_{\text{unsteady aero}} \right) \tag{5}$$

$s_r$ is defined as $s_r := s\frac{c_{\text{ref}}}{2V}$, where $s$ is the Laplace variable. $A_0, A_{1s}$ are the static deflections and velocity dependence terms respectively for steady aerodynamics. $A_{1us}, A_2$ are the quasi-steady and acceleration terms for unsteady aerodynamics. $A_l$ represents the aerodynamic lag term coefficients and $b_l$ are the corresponding poles which are picked a priori to simplify the fitting process. By substituting $s_r = ik$ in Eq. (5), the DLM solution at the reduced frequency $k$ may be obtained. Also, using the relation between $s_r$ and $s$ stated above, the aerodynamic model in Eq. (5) can be expressed as a MIMO transfer function for a given airspeed $V$ (denoted as $A_V(s)$). Thus, a linear aerodynamic model is obtained which is parametrically dependent on the airspeed $V$.

The fitting can be visualized in Fig. 5 which shows the transfer function from vertical velocity input to the resulting first wing bending force evaluated at the airspeed $V = 20\,\text{m/s}$. The associated fitting errors serve as an important source of modeling uncertainty and are described in the later sections. Equations (3) and (4) can be combined by eliminating the forcing terms to define the nominal aeroelastic model in Laplace domain as

$$\left[Ms^2 + Cs + K - \bar{q} A_V(s)\right] \begin{bmatrix} \eta_r \\ \eta_s \end{bmatrix} = 0 \tag{6}$$

Here, $A_V(s)$ represents the continuous aerodynamic model in Eq. (5) evaluated at a given airspeed $V$. Equation 6 describes the nominal aeroelastic model in which modeling uncertainties can be included, as described in the next section.

## III. Robust Flutter Analysis

This section covers the concept of robust flutter analysis for uncertain systems and the associated mathematical tools. First, flutter analysis for the nominal model developed in the previous section is presented, followed by the conceptual description of uncertainty modeling for the aeroelastic model. This is followed by a brief overview of the $\mu$ framework for uncertain systems. Finally, a graphical approach is presented for calculating the robust flutter boundary for in the $\mu$ framework.

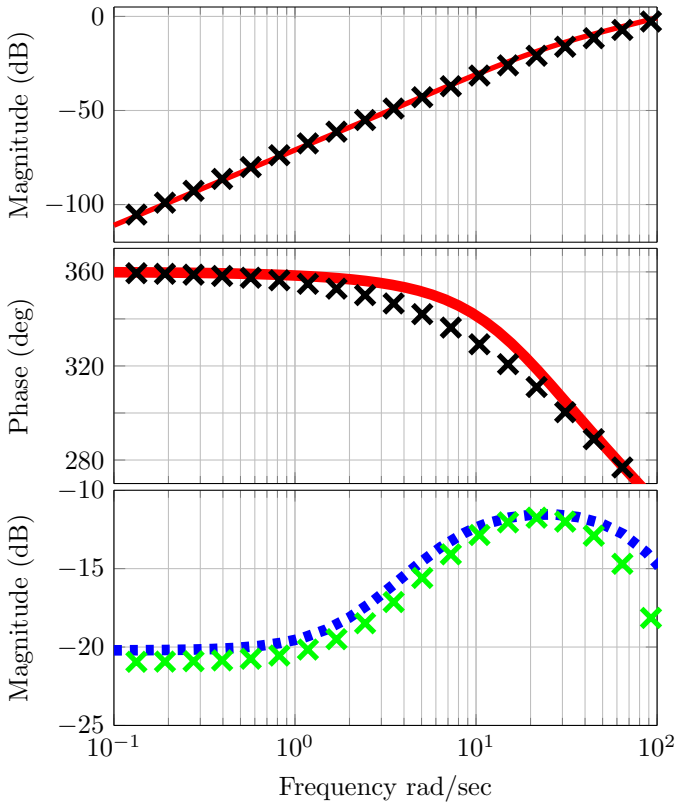


**Figure 5. Least squares fit for aerodynamics given by ( ), raw DLM data: ( ), fitting errors: ( ) and the upper bound on the errors: ( )**

### A. Flutter Analysis

Flutter boundary is defined as the flight condition at which there is onset of flutter.[1,18] If the aircraft is assumed to be in straight and level flight at constant altitude, the flutter boundary is essentially the smallest airspeed at which flutter occurs. In this paper the flutter boundary is only calculated under these conditions. It should be noted that Eq. (6) is a general representation of aeroelastic models with a linear structural model and linear unsteady aerodynamics.[1,2] By computing eigenvalues associated with the model at a given airspeed, stability of the system can be determined. The eigenvalues of the system will be complex conjugates of the form

$$\lambda = -\zeta\omega_n \pm i\omega_n\sqrt{1-\zeta^2} \tag{7}$$

where $\zeta$ is the damping ratio and $\omega_n$ is the natural frequency for a given eigenmode. The non-zero damping ratios of eigenmodes determine their decaying or rising amplitudes which correspond to their stability or instability. If (as noted in the previous section) the aerodynamics model is available only as a complex valued matrix at discrete frequencies for a simple harmonic oscillation, the frequency has to be chosen a priori to solve Eq. (6) for the eigenvalues of the system. However, the appropriate frequency for the aerodynamics model is the frequency of the eigenmode whose stability is of interest, which is not known a priori. Another inconsistency is that the aerodynamic model is only valid for simple harmonic modes with no damping effects. Historically, this problem has been solved by using iterative methods for choosing the appropriate frequency and approximations regarding the true aerodynamic forces on a damped oscillating system. For example, the 'p-k' method assumes the aerodynamic model for simple harmonic oscillations to be a good approximation for a system with lightly damped modes.[32] The 'g' method on the other hand makes a first order approximation to get an aerodynamic model for damped oscillations based on the available model for simple harmonic oscillations.[33]

In this paper, the aerodynamic model at a given airspeed is obtained as a continuous model in the Laplace domain ($A_V(s)$) via a rational function approximation. Therefore the entire system can be directly solved for the eigenmodes like any typical linear system. However it should be kept in mind that the aerodynamic model $A_V(s)$ is strictly valid only for $s = i\omega$ (or equivalently, $A(s_r)$ is valid only for $s_r = ik$). That is to

say, it is only valid for sinusoidal inputs at a given frequency $\omega$. Hence by directly solving for eigenmodes, we make an approximation equivalent to that in the p-k method. The rational function fitting simply helps avoid the iterative process for choosing the appropriate oscillating frequency for aerodynamics and also helps provide a continuous model for time domain simulations if necessary.

To calculate the flutter boundary for body freedom flutter, we track the eigenmodes of the system in Eq. (6) associated with first wing bending and short period across a grid of airspeeds. The variation of short period and first symmetric wing bending modes with respect to airspeed is shown in Fig. 6. The first wing

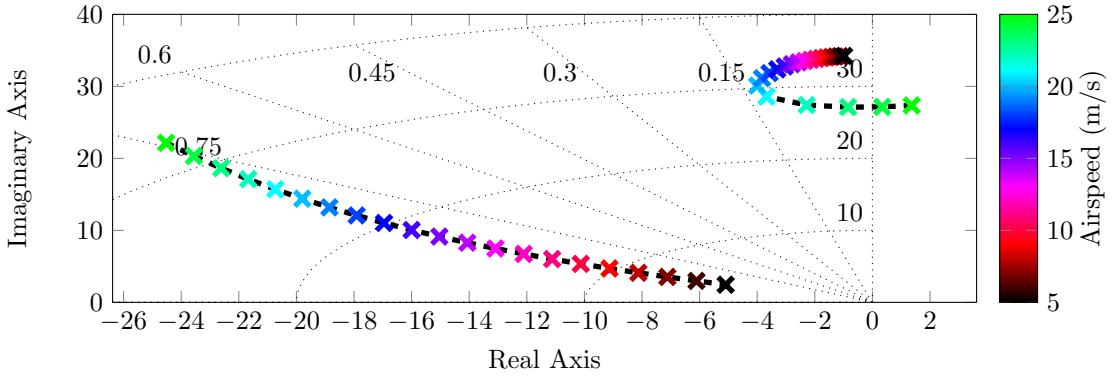


**Figure 6. Short period and first symmetric wing bending modes variation with airspeed**

bending mode goes unstable between 23 and 24 m/s. A closer search between that interval gives the flutter speed to be 23.8 m/s. This flutter boundary will be referred to as the nominal flutter boundary, since it is associated with the nominal model which has no uncertainties. Next, we will discuss the model uncertainties which will be accounted for, and then outline the procedure for obtaining a robust flutter boundary with respect to the uncertain model.

## B. Uncertainty Description

Uncertainties and modeling errors in the aeroelastic model can arise from different sources like-

1. Parametric uncertainties in structural properties (mass and material properties) obtained from experimental data and used in the structural model.
2. Parametric uncertainties in steady aerodynamics model.
3. Unmodeled dynamics in the incremental unsteady aerodynamics model obtained from the DLM.
4. Nonlinearities ignored in linearization procedures or hard nonlinearities like saturation in components such as actuators.

This paper considers the first three types listed above, using the linear robust control framework based on $\mu$. The nonlinearities can be addressed using the more general Integral Quadratic Constraints framework[22] in the future, although nature of the analysis will remain the same. Similar use of IQCs for robustness analysis of aeroservoelastic systems can be seen in literature.[23,24] Since all the uncertainties are specified at a subsystem level, it is possible to build uncertain subsystems and then connect them suitably to obtain the overall model. Also, the parametric and dynamic uncertainties specified for individual parameters such as stiffness parameters or unsteady part of aerodynamics can be pulled out and grouped together in a linear fractional transformation (LFT)[16] interconnection. The uncertain subsystems can then be connected as shown in Fig. 7. $S_{22}$ is the combined rigid body - structural dynamics nominal model described in Eq. (3) and $A_{V_{11}}$ is the nominal aerodynamic model $A(s_r)$ as given in Eq. (5), evaluated at a given airspeed $V$. All the other blocks $S_{ij}$ and $A_{V_{ij}}$ represent the effects of uncertainties on the corresponding subsystems. The block $\Delta_s$ is a structured uncertainty consisting of parametric uncertainties related to mass properties and structural stiffness properties. Similarly, $\Delta_a$ consists of the parametric and dynamic uncertainties associated with steady and unsteady aerodynamics respectively. Further details on these uncertainties are discussed

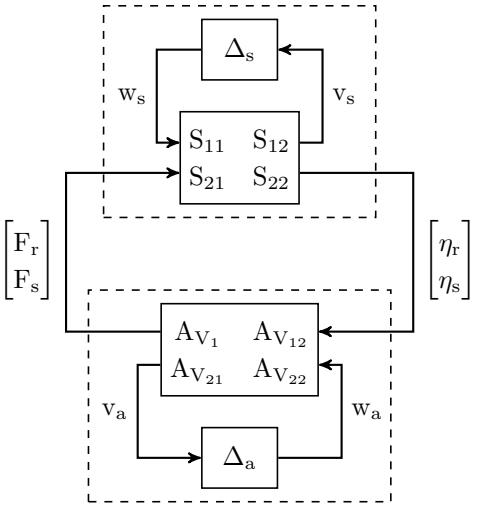


**Figure 7. Aeroelastic model with subsystem based uncertainties**

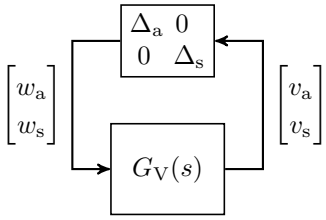


**Figure 8. Simplified Aeroelastic model with Structured Uncertainty**

in the next section. These uncertainty blocks can be collected into a unified structured uncertainty $\Delta$, in a closed loop around the overall model represented by $G_V(s)$ as shown in Fig. 8.

$G_V(s)$ contains the entire aeroelastic model along with the uncertainty interaction terms shown in Fig. 7. These LFT block diagram manipulations can be performed conveniently using commercially available software. In this paper, these manipulations and all computations associated with $\mu$ analysis are done using the robust control toolbox in MATLAB.[34]

### C. Robust Stability Analysis Using $\mu$

For the uncertain system in Fig. 8, given both $G_V(s)$ and the uncertainty $\Delta \in \mathbf{\Delta}$ are internally stable systems, where $\mathbf{\Delta}$ is the set of all block structured uncertainties considered for this analysis, the closed loop is stable for all allowed $\Delta$ if and only if

$$\det(I - G_V(i\omega)\Delta) \neq 0 \quad \forall\omega\forall\Delta \in \mathbf{\Delta} \tag{8}$$

Equation (8) follows from the Nyquist stability theorem applied to a feedback system with a stable open loop transfer function.[16] Based on this stability condition a measure of robustness called the structured singular value $\mu$ is defined for a given frequency $\omega$ and $\Delta \in \mathbf{\Delta}$ as

$$\mu_\Delta(G_V(i\omega)) = \frac{1}{\min\{K|\ \det(I - G_V(i\omega)K\Delta) = 0, \bar{\sigma}(\Delta) \leq 1\}} \tag{9}$$

Thus, $\mu$ is defined as the inverse of the minimum scaling factor $K$ for which $(I - G_V\Delta)$ is singular at a given frequency $\omega$, where $\Delta$ is norm-bounded. The norm boundedness of $\Delta$ can be achieved via suitable rescaling of $G_V$. The scaling factor $K$ can be considered to be analogous to robustness margin of $G_V(i\omega)$ at a given frequency $\omega$. Based on Eq. (9), a robust stability condition can now be written as

$$\mu_\Delta(G_V(i\omega)) < 1 \quad \forall\omega\forall\Delta \in \mathbf{\Delta}, \bar{\sigma}(\Delta) \leq 1 \tag{10}$$

It basically states that if the minimum scaling $K$ required for the closed loop to become unstable is greater than unity for all frequencies, then the system is robustly stable for all norm bounded structured uncertainty $\Delta \in \mathbf{\Delta}$. Typically, Eq. (9) is computed on a frequency grid which is specified across a given frequency range of interest for the system at hand. The condition in Eq. (10) can then be checked at these frequency points for robust stability. For an aeroelastic model, a robust flutter boundary can thus be computed based on this robust stability condition.

### D. Robust Flutter Boundary Computation

A Robust flutter boundary can be considered as the smallest airspeed at which an uncertain aeroelastic system shown in Fig. 8 becomes unstable. Going by the condition in Eq. (10) for robust stability, a robust flutter boundary can be computed as the airspeed $V_{\text{rfb}}$ at which the maximum occurring $\mu_\Delta G_V(i\omega)$ across a specified frequency range is equal to unity. Thus, for a given set of block structured uncertainties $\mathbf{\Delta}$, $V_{\text{rfb}}$ is defined as the smallest airspeed $V$ such that

$$\max_{\omega \in \mathbf{\Omega}} \mu_\Delta G_V(i\omega) = 1 \tag{11}$$

Here $\mathbf{\Omega}$ represents the frequency grid specified across the desired frequency range for the analysis. In other words, for all airspeeds $V < V_{\text{rfb}}$, the robust stability condition specified by Eq. (10) is satisfied, and gets violated at $V_{\text{rfb}}$ for the first time at some frequency. $V_{\text{rfb}}$ can be obtained graphically as described ahead.

For a given frequency grid $\mathbf{\Omega}$ and airspeed $V$, compute instability scaling factor $\bar{\text{K}}$ as

$$\bar{K} = \frac{1}{\max\limits_{\omega \in \mathbf{\Omega}} \ \mu_\Delta(G_V(i\omega))} \tag{12}$$

Note that $\bar{\text{K}}$ is simply the inverse of the value of maximum $\mu_\Delta(G_V)$ occurring over $\mathbf{\Omega}$ at a given airspeed. $\bar{\text{K}}$ can be computed for a range of airspeeds and plotted on a $\bar{\text{K}} - \text{V}$ graph. The $\bar{\text{K}} - \text{V}$ graph has been developed as the primary tool for computing robust fluter boundary in this analysis. From Eq. (11) it can be seen that the point where this plot intersects $\bar{\text{K}} = 1$ line on the graph corresponds to the robust flutter boundary. Fig. 9 shows a typical graph which shows the robust flutter boundary. Although we can just as

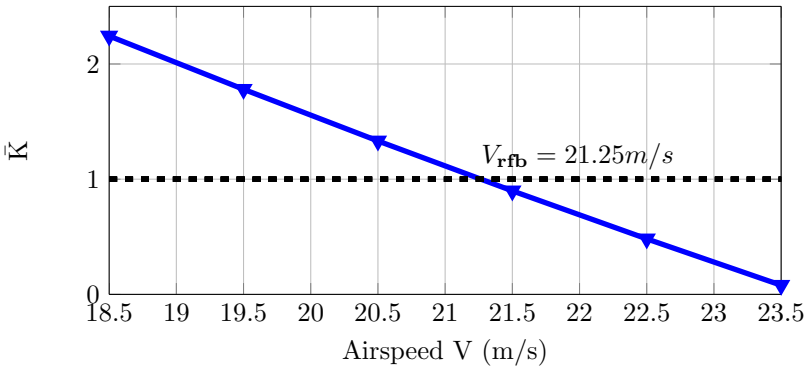


**Figure 9. An example of a $\bar{\text{K}} - \text{V}$ graph**

easily plot the maximum $\mu_\Delta(G_V)$ instead of its inverse $\bar{\text{K}}$, $\bar{\text{K}} - \text{V}$ graph seems to be more intuitive since $\bar{\text{K}}$ is analogous to robustness margin. It is easy to see how much scaling of the uncertainty would make the aeroelastic system unstable at any given airspeed. For example, at an airspeed of $V = 19\,\text{m/s}$, Fig. 9 shows that the specified uncertainty bounds need to be doubled for the aeroelastic system to go unstable. On the other hand, the bounds will need to be scaled to 50% if the aircraft needs to be stable at $V = 22.5\,\text{m/s}$. Also, as $\bar{\text{K}}$ approaches zero on the right end of the Fig. 9, it will intersect the $x$ axis at the nominal flutter speed of the system. This is because at the nominal flutter speed, the system would be unstable at flutter frequency even if $\Delta$ is set to zero i.e. zero uncertainty. Therefore the corresponding value for $\mu_\Delta(G_V)$ would be infinite at the flutter frequency (which means $\bar{\text{K}} = 0$) . Therefore by graphically extrapolating the $\bar{\text{K}} - \text{V}$ graph, nominal flutter speed can be estimated in an alternate manner.

## IV. Sensitivity Analysis

For sensitivity analysis, a baseline uncertain model is built where different sources of model uncertainties are considered. The objective is to study the affect of each individual uncertainty on the robust flutter boundary as it is scaled up relative to others. Most uncertainties are parametric in nature and hence embedded in the model when constructed. They are pulled out into the overall structured uncertainty block as shown in Fig. 8 using the *lftdata* command in the robust control toolbox.[34] A sensitivity scaling parameter is defined for each of these uncertainties, which facilitates their individual scaling. This parameter varies from 0.6 to 2, the baseline value being 1. Thus, it scales the baseline uncertainty between 60% and 200%. The uncertainties are listed below along with their baseline bounds.

1. **Real parametric uncertainty for steady aerodynamics coefficients:** $C_{L\alpha}$, $C_{Lq}$, $C_{M\alpha}$ and $C_{Mq}$ have been modeled with parametric bounded uncertainty. These coefficients are isolated from the steady part of the aerodynamics model shown in Eq. (5) and multiplicative uncertainty is incorporated so that the uncertain coefficients are

$$C_{X_{\text{unc}}} = C_{X_{\text{nom}}}(1 + k_{\text{Xsens}} W_{C_X} \delta_{C_X}) \quad \text{where } X \in \{L\alpha, Lq, M\alpha, Mq\} \tag{13}$$

   $C_{X_{\text{nom}}}$ is the nominal value of the coefficient in consideration, $\delta_{C_X}$ is a norm bounded real valued uncertainty ($|\delta_{C_x}| \leq 1$), $W_{C_X}$ is the baseline uncertainty bound required for each coefficient and $k_{\text{Xsens}}$ is the sensitivity scaling, which is unity for the baseline uncertain model. For the lift coefficients, $W_{L\alpha}$ and $W_{Lq}$ are set to 0.1, which corresponds to $\pm 10\%$ uncertainty about the nominal value. For pitching moment coefficients, $W_{M\alpha}$ and $W_{Mq}$ are set to 0.05 or $\pm 5\%$ uncertainty. These bounds are chosen by looking at the overall variation in values of the mentioned coefficients obtained from various sources such as potential flow based panel methods (in-house as well as popular open source codes like TORNADO (`tornado.redhammer.se`) and XFOIL (`xflr5.com`), computational fluid dynamics[35] and wind tunnel tests.

2. **Real parametric uncertainty for moments of inertia:** Moments of inertia about the three axes are obtained via inertia swing tests.[14] The measurement errors in these tests have been estimated and documented, and they form the basis for specifying real parametric uncertainty bounds. The uncertainty is incorporated as a multiplicative uncertainty on each of the inertia values to get

$$I_{m_{\text{unc}}} = I_{m_{\text{nom}}}(1 + k_{\text{Imsens}} W_{\text{Im}} \delta_{\text{Im}}) \quad \text{where } I_m \in \{I_{xx}, I_{yy}, I_{zz}\} \tag{14}$$

   $I_{m_{\text{nom}}}$ represents the nominal value of each of the inertias, $\delta_{\text{Im}}$ is a norm bounded real valued uncertainty, $W_{\text{Im}}$ is the baseline bound and $k_{\text{Imsens}}$ is the sensitivity scaling parameter. The baseline bounds for all three moments of inertia are chosen to be 0.05 or $\pm 5\%$ based on measurement errors. The rigid mass matrix $M_r$ in Eq. (3) is constructed using these uncertain inertia values.

3. **Real parametric uncertainty for structural stiffness properties:** Young's modulus and shear modulus of the Euler beams in the finite element model for the wings section have been estimated via a series of static and ground vibration tests.[14] The experimental errors in these tests are accounted for via real parametric uncertainties to get

$$X_{\text{unc}} = X_{\text{nom}}(1 + k_{\text{Ssens}} W_S \delta_S) \tag{15}$$

   $X_{\text{nom}}$ represents the nominal value of each of the moduli, $\delta_S$ is a norm bounded real valued uncertainty, $W_S$ is the baseline bound and $k_{\text{Ssens}}$ is the sensitivity scaling parameter. The bounds for both moduli are chosen as 0.1 or $\pm 10\%$ based on the estimated experimental errors. The stiffness matrix $K_s$ in Eq. (2) is constructed from these uncertain moduli using standard finite element techniques.[9,28]

4. **Dynamic uncertainty in unsteady aerodynamics:** The dynamic uncertainty in unsteady aerodynamics is modeled as a LTI system uncertainty which bounds the least square fitting errors of the rational function approximation. The fitted model is considered nominal and its deviation from raw data (from DLM) is used to compute the uncertainty upper bound. From Eq. (5) we see that nominal unsteady aerodynamics can be described as a rational function as

$$UA_{\text{nom}} = A_{1us} s_r + A_2 {s_r}^2 + \sum_{l=1}^{n} A_l \frac{s_r}{s_r + b_l} \tag{16}$$

The uncertainty is described as an output multiplicative uncertainty based on the nominal model and a scalar LTI uncertain block $\Delta_{\text{dyn}}$ which has a gain bound of unity.

$$UA_{\text{unc}} = (I + k_{\text{dyn}} W_{\text{dyn}} \Delta_{\text{dyn}}) UA_{\text{nom}} \tag{17}$$

$k_{\text{dyn}}$ is the sensitivity scaling parameter, $W_{\text{dyn}}$ is the weighting function for the dynamic uncertainty which provides a conservative upper bound on the fitting errors, as shown in Fig. 5. It is computed by first fitting the discrete error magnitudes to a transfer function (MATLAB command $fitmagfrd$). The resulting transfer function is then increased in magnitude by 5% to obtain $W_{\text{dyn}}$. This is done to ensure that the weight is a slightly conservative upper bound to the fitting errors. $W_{\text{dyn}}$ has the same dimensions as the aerodynamic model and is constructed as shown for each input-output combination of the aerodynamic model. It gives an insight on the variation of fitting errors with frequency. It can be seen that error magnitude rises in the frequency range close to the lag states poles which are chosen a priori. The error in choosing these poles is considered a systemic error, not accounted for in the baseline model. They are a part of the scaled up analysis.

5. **Dynamic uncertainty for location of center of gravity:** Location of center of gravity (C.G.) is obtained experimentally along with its corresponding measurement errors.[14] The baseline uncertainty in its location is assumed to be $\pm 0.05m$. This uncertainty (assuming total mass remains constant) is primarily reflected in the structural mass matrix of the finite element model. This affects the mode shapes of the aircraft and therefore all the modal mass, damping and stiffness matrices as well as the aerodynamic model which is transformed into modal coordinates. Therefore, to account for the effects due to the baseline uncertainty specified above, a dynamic uncertainty is assumed for the overall aerodynamic and structural subsystem models. The corresponding upper bounds $W_{\text{Acg}}$ and $W_{\text{Scg}}$ for these uncertainties are estimated by finding the difference between the nominal aerodynamic and structural models from Eqs. (**??**) and (3) and the models obtained by moving the C.G. by the maximum baseline value. The uncertain subsystem models are defined as

$$\begin{aligned} A_{\text{unc}} &= (I + k_{\text{cg}} W_{\text{Acg}} \Delta_{\text{cg}}) A_{\text{nom}} \\ S_{\text{unc}} &= (I + k_{\text{cg}} W_{\text{Scg}} \Delta_{\text{cg}}) S_{\text{nom}} \end{aligned} \tag{18}$$

$A_{\text{nom}}$ and $S_{\text{nom}}$ are the aerodynamic and structural models with C.G. at nominal location and $k_{\text{cg}}$ is the sensitivity scaling parameter. The resulting uncertain models $A_{\text{unc}}$ and $S_{\text{unc}}$ are integrated with other uncertainties listed above. Although this approach may not be conservative enough compared to a real parametric uncertainty specification for C.G. location, it is far less computationally intensive.

Equations (13) - (18) provide the uncertain parameters and uncertain dynamics, which can then scaled individually for sensitivity analysis via the sensitivity scaling parameters. The results of the analysis are discussed ahead.

## A. Results

The range of scaling factors are kept the same for each uncertainty bound, between 60% and 200%. This is analogous to the skewed-$\mu$ problem. A $\bar{\text{K}} - \text{V}$ graph can be plotted after each uncertainty is scaled up individually. As an example, the stiffness sensitivity scaling parameter $k_{\text{Ssens}}$ is scaled between 0.6 and 2 (or 60% and 200%) and the $\bar{\text{K}} - \text{V}$ graph is plotted for each scaled value as shown in Fig. 10.

Note that $\bar{\text{K}}$ refers to the scaling of the overall uncertainty $\Delta$ required for instability, whereas $k_{\text{Ssens}}$ refers to the skewed scaling of uncertainty $\delta_S$ associated with stiffness properties only. The flutter speed as defined earlier, is the airspeed at which the $\bar{\text{K}} - \text{V}$ line intersects the $\bar{\text{K}} = 1$ line. We see in Fig. 10 that with increase in $k_{\text{Ssens}}$, the robust flutter boundary $V_{\text{rfb}}$ decreases, which is as expected since the overall uncertainty is increases. This variation can be visualized via a sensitivity graph where $V_{\text{rfb}}$ is plotted against the corresponding sensitivity parameter. The same process can be used for uncertainties associated with estimated moments of inertia, location of C.G., steady and unsteady aerodynamics. From the $\bar{\text{K}} - \text{V}$ graphs associated with all uncertainties, we can pull out the variation of flutter speeds with their corresponding sensitivity scaling factors. A sensitivity graph can then be plotted which shows this variation for each uncertainty as shown in Fig. 11. Fig. 11 shows how the robust flutter boundary varies as each uncertainty is scaled individually. Since all the scalings are between 60% and 200%, all the variations can be plotted and compared on a single graph.

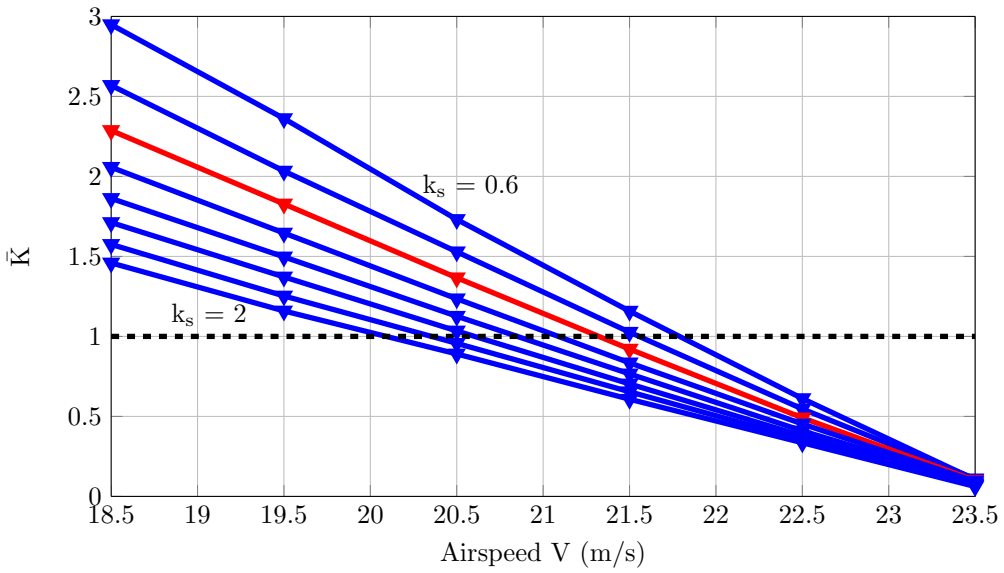


**Figure 10. $\bar{K} - V$ graph variation in uncertainty for structural stiffness, baseline uncertainty given by (▼)**

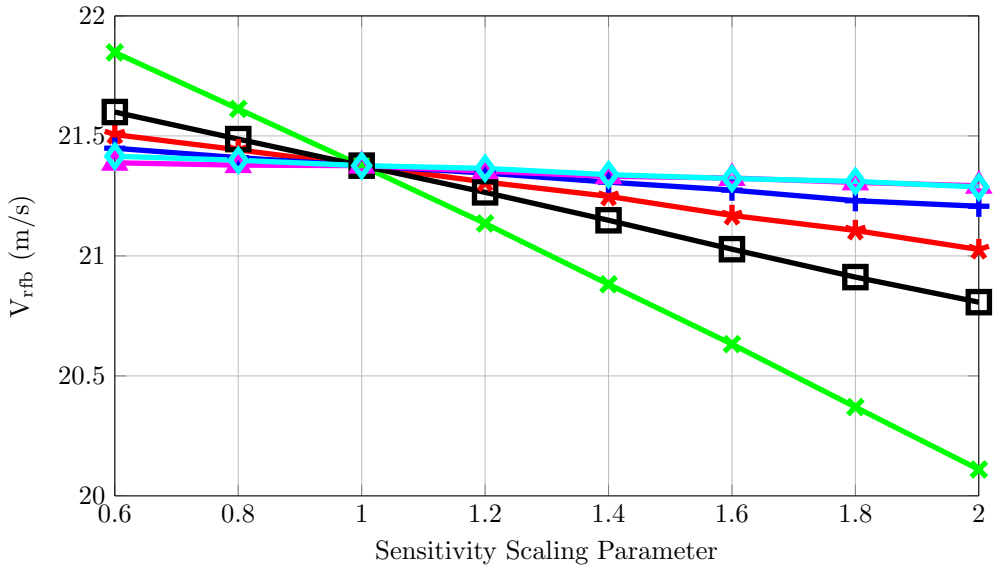


**Figure 11. The lines represent steady lift coeff: (+), steady pitch coeff: (▲), unsteady aerodynamics: (✱), moment of inertia: (◇), structural stiffness: (×), and C.G. location: (□)**

## B. Discussion and Future Work

Fig. 11 provides insight into the relative sensitivities of different uncertainties. The plots all intersect at the baseline uncertainty where all sensitivity scalings are unity. This point represents the baseline robust flutter boundary $V_{\text{rfb}} = 21.37\,\text{m/s}$. This is the minimum airspeed beyond which the baseline uncertain model becomes unstable. But as various uncertainties are scaled individually, Fig. 11 clearly shows that $V_{\text{rfb}}$ is most sensitive to the structural stiffness estimation. This is followed by the dynamic uncertainty due to C.G. variation and unsteady aerodynamics. However, the flutter boundary seems to be highly unaffected by uncertainties in either steady aerodynamics pitch coefficient or moments of inertia and only marginally affected by the steady lift coefficient uncertainty. We can compute the average slopes of each line in Fig. 11 and normalize them with the lowest value which gives a quantitative idea of relative sensitivity of the various uncertainties. The slope values are listed in Table 2.

Thus, we see that sensitivity to stiffness properties is twice the next highest value corresponding to C.G.

**Table 2. Slopes of the Sensitivity Plot for different Uncertainties**

| Uncertainty | Source | Slope | Norm. Slope |
|---|---|---|---|
| $\delta_s$ | Structural Stiffness | -1.24 | 18.12 |
| $\delta_{\text{Im}}$ | Moments of Inertia | -0.09 | 1.34 |
| $\Delta_{\text{cg}}$ | Center of Gravity | -0.56 | 8.88 |
| $\delta_{C_M}$ | Pitching moment Coeff | -0.068 | 1 |
| $\delta_{C_L}$ | Steady Lift Coeff | -0.17 | 2.52 |
| $\Delta_{\text{dyn}}$ | Unsteady Aerodynamics | -0.34 | 4.99 |

location uncertainty and 18 times more sensitive than the lowest value, that of pitching moment coefficient. Of course, these results are highly dependent on the baseline bounds assumed for each uncertainty. For example, the baseline bound $W_{C_L}$ assumed for $C_L$ coefficients is $\pm 10\%$, which is then scaled by a factor of 0.6 to 2. Therefore in the absolute sense, the bound is varied from $\pm 6\%$ to $\pm 20\%$. However, if the baseline bound is assumed at, say, $\pm 50\%$, then the same scaling range results in the bound varying from $\pm 30\%$ to $\pm 100\%$ in the absolute sense. This leads to a greater drop in robust flutter boundary for the same scaling. So if baseline bounds for a particular uncertainty is raised relative to others, then for the same scaling range, that uncertainty will appear to be more sensitive on this graph. Hence, for this comparison to be valid, baseline bounds have to be selected carefully.

In the case of structural stiffness parameters (Young's and Shear Modulus), as the bounds on the corresponding uncertainties is tightened via better experimental measurements, we can push the robust flutter boundary closer to the nominal boundary far more compared to other uncertainties. Conversely, a poor experimental accuracy can cause $V_{\text{rfb}}$ to drop rapidly since the baseline bound itself increases.

Next, variation of uncertainty in the location of center of gravity affects $V_{\text{rfb}}$ significantly. However, the experimental measurement for this parameter is very accurate.[14] Even the baseline uncertainty assumed has very large bounds, thus contributing to the high sensitivity. However, in aircraft with varying C.G. location (typically due to fuel burn), the model may not to be able to predict the location as accurately as ground tests. This provides significant scope for uncertainty in C.G. location. In such a scenario, it becomes very important to keep the modeling error low since the analysis reveals high sensitivity to C.G. location. Also, we need to keep in mind that the uncertainty description in this case may not be conservative enough, so the sensitivity could be potentially higher. It is an open problem to be addressed in future work.

Although the flutter boundary is less sensitive to unsteady aerodynamics, it is the only aspect of this model which is obtained purely from a single theoretical approach. Although the DLM itself has been validated against experimental data,[29] there is no experimental data to either validate the unsteady aerodynamics model for this aircraft or to provide bounds on it. As mentioned earlier, the baseline error bounds are specified based on fitting errors only, although there could potentially be significant discrepancy at the baseline level itself. Thus, given its relatively high sensitivity, as well as the fact that the model is not verified or bounded via experimental data, it serves as one of the most important areas for further investigation.

The steady aerodynamics and moments of inertia seem to be of little significance to flutter prediction that therefore can be estimated as being done currently. Also, we can assume they do not play a significant role in any observed deviation from flight test data. This methodology for sensitivity analysis can be extended to compare effects of uncertainty on various input-output performance metrics. In future, a similar approach will be used to study the effects of various uncertainties on gust response, handling qualities and control surface effectiveness. Also, in the near future, integral quadratic constraints[22] will be incorporated to include nonlinearities such as actuator saturation and neglected higher order terms.[36] Finally, this framework will also be used for model updating from flight test data. It is envisioned that these analyses will enable a least conservative uncertain model which effectively represent any variations of flight data from the nominal model, since it will be known a priori which sources of uncertainties and nonlinearities are most influential for stability and performance of the aeroelastic system.

## Acknowledgments

We would like to acknowledge NASA NRA, "Lightweight Adaptive Aeroelastic Wing for Enhanced Performance Across the Flight Envelope," NRA NNX14AL36A, Mr. John Bosworth Technical Monitor, Mr.

Dan Moerder acting Technical Monitor, for funding this research. The authors also acknowledge the PAAW research group for valuable and fruitful discussions and insights into various aspects of aeroservoelasticity.

## References

[1]Cox, D., Curtiss Jr, H., Edwards, J., Hall, K., Peters, D. A., Scanlan, R., Simiu, E., and Sisto, F., *A modern course in aeroelasticity*, Vol. 116, Springer, 2006.

[2]Fung, Y. C., *An introduction to the theory of aeroelasticity*, Courier Dover Publications, 2002.

[3]Kotikalpudi, A., Pfifer, H., and Balas, G. J., "Unsteady Aerodynamics Modeling for a Flexible Unmanned Air Vehicle," *AIAA Atmospheric Flight Mechanics Conference*, 2015, p. 2854.

[4]Kotikalpudi, A., Moreno, C., Taylor, B., Pfifer, H., and Balas, G. J., "Low cost development of a nonlinear simulation for a flexible uninhabited air vehicle," *American Control Conference*, 2014, pp. 2029–2034.

[5]Moreno, C., Seiler, P., and Balas, G., "Linear parameter varying model reduction for aeroservoelastic systems," *AIAA Atmospheric Flight Mechanics Conference*, 2012, p. 4859.

[6]Theis, J., Takarics, B., Pfifer, H., Balas, G., and Werner, H., "Modal Matching for LPV Model Reduction of Aeroservoelastic Vehicles," *AIAA Science and Technology Forum*, 2015.

[7]Wang, S., Pfifer, H., and Seiler, P., "Robust synthesis for linear parameter varying systems using integral quadratic constraints," *Conference on Decision and Control*, IEEE, 2014, pp. 4789–4794.

[8]Theis, J., Pfifer, H., and Seiler, P., "Robust Control Design for Active Flutter Suppression," *AIAA Atmospheric Flight Mechanics Conference*, 2016.

[9]Moreno, C. P., Gupta, A., Pfifer, H., Taylor, B., and Balas, G. J., "Structural model identification of a small flexible aircraft," *American Control Conference*, 2014, pp. 4379–4384.

[10]Gupta, A., Moreno, C., Pfifer, H., Taylor, B., and Balas, G., "Updating a finite element based structural model of a smalll flexible aircraft," *AIAA Scitech Conference*, 2015.

[11]Dorobantu, A., Johnson, W., Lie, F. A., Taylor, B., Murch, A., Paw, Y. C., Gebre-Egziabher, D., and Balas, G., "An airborne experimental test platform: From theory to flight," *American Control Conference 2013*, 2013, pp. 659–673.

[12]Dorobantu, A., Murch, A., Mettler, B., and Balas, G., "System identification for small, low-cost, fixed-wing unmanned aircraft," *Journal of Aircraft*, Vol. 50, No. 4, 2013, pp. 1117–1130.

[13]Pfifer, H. and Danowsky, B., "System Identification of a Small Flexible Aircraft," *AIAA Atmospheric Flight Mechanics Conference*, 2016.

[14]Regan, C. and Taylor, B., "mAEWing1: Design, Build test," *AIAA Atmospheric Flight Mechanics Conference*, 2016.

[15]Zhou, K., Doyle, J. C., and Glover, K., *Robust and optimal control*, Vol. 40, Prentice hall New Jersey, 1996.

[16]Skogestad, S. and Postlethwaite, I., *Multivariable feedback control: analysis and design*, Vol. 2, Wiley New York, 2007.

[17]Borglund, D., "The mu-k method for robust flutter solutions," *Journal of Aircraft*, Vol. 41, No. 5, 2004, pp. 1209–1216.

[18]Lind, R. and Brenner, M., *Robust aeroservoelastic stability analysis: Flight test applications*, Springer Science & Business Media, 2012.

[19]Lind, R. and Brenner, M., "Flutterometer: an on-line tool to predict robust flutter margins," *Journal of Aircraft*, Vol. 37, No. 6, 2000, pp. 1105–1112.

[20]Ferreres, G., *A practical approach to robustness analysis with aeronautical applications*, Springer Science & Business Media, 1999.

[21]Ferreres, G., Biannic, J., and Magni, "A skew mu toolbox (SMT) for robustness analysis," *International Symposium on Computer Aided Control Systems Design*, IEEE, 2004, pp. 309–314.

[22]Megretski, A. and Rantzer, A., "System analysis via integral quadratic constraints," *IEEE Transactions on Automatic Control*, Vol. 42, No. 6, 1997, pp. 819–830.

[23]Vuillemin, P., Demourant, F., Biannic, J.-M., and Poussot-Vassal, C., "Global stability validation of an uncertain large-scale aircraft model," *Conference on Control Applications (CCA)*, IEEE, 2014, pp. 152–157.

[24]Demourant, F., "New algorithmic approach based on integral quadratic constraints for stability analysis of high order models," *European Control Conference (ECC)*, IEEE, 2013, pp. 359–364.

[25]Burnett, E., Atkinson, C., Beranek, J., Sibbitt, B., Holm-Hansen, B., and Nicolai, L., "NDOF Simulation model for flight control development with flight test correlation," *AIAA Modeling and Simulation Technologies Conference*, Vol. 3, 2010, pp. 7780–7794.

[26]Creech, G., "Introducing the X-56A MUTT: Who Let the Dog Out?" *Online at: www.nasa.gov/topics/aeronautics/features/x − 56a_mutt.html*.

[27]Waszak, M. R. and Schmidt, D. K., "Flight dynamics of aeroelastic vehicles," *Journal of Aircraft*, Vol. 25, No. 6, 1988, pp. 563–571.

[28]Zienkiewicz, O. C. and Morice, P., *The finite element method in engineering science*, McGraw-hill, 1971.

[29]Albano, E. and Rodden, W. P., "A doublet-lattice method for calculating lift distributions on oscillating surfaces in subsonic flows." *AIAA Journal of Aircraft*, Vol. 7, No. 2, 1969, pp. 279–285.

[30]Blair, M., "A compilation of the mathematics leading to the doublet lattice method," Tech. rep., DTIC Document, 1992.

[31]Kier, T. and Looye, G., "Unifying manoeuvre and gust loads analysis models," *International Forum on Aeroelasticity & Structural Dynamics*, 2009.

[32]Hassig, H. J., "An approximate true damping solution of the flutter equation by determinant iteration." *Journal of Aircraft*, Vol. 8, No. 11, 1971, pp. 885–889.

[33]Chen, P., "Damping perturbation method for flutter solution: the g-method," *AIAA journal*, Vol. 38, No. 9, 2000, pp. 1519–1524.

[34]Balas, G., Chiang, R., Packard, A., and Safonov, M., "Robust control toolbox," *For Use with Matlab. Users Guide, Version*, Vol. 3, 2005.

[35]Farhat, C., Lesoinne, M., and Le Tallec, P., "Load and motion transfer algorithms for fluid/structure interaction problems with non-matching discrete interfaces: Momentum and energy conservation, optimal discretization and application to aeroelasticity," *Computer methods in applied mechanics and engineering*, Vol. 157, No. 1, 1998, pp. 95–114.

[36]Takarics, B. and Seiler, P., "Gain scheduling for nonlinear systems via integral quadratic constraints," *American Control Conference*, 2015.